Russian Physics Journal, Vol. 57, No. 10, February, 2015 (Russian Original No. 10, October, 2014)

REACTION SINTERING OF POROUS SHAPE-MEMORY TITANIUM–NICKELIDE-BASED ALLOYS

N. V. Artyukhova,[1] Yu. F. Yasenchuk,[1] Kim Ji-Soon,[2] and V. É. Gunther[1] UDC 621.762

The problems of reaction sintering of porous shape-memory Ti–Ni*-based alloys are examined. An analysis of the structure and parameters of shape-memory materials produced with the use of different reaction sintering modes is performed. The temperature and time intervals are determined over which liquid-phase sintering points responsible for a qualitative change in the* TiNi *phase of the reaction-sintered* Ti–Ni system are *observed. The morphological structure and properties of the porous materials are investigated. Models for interactions between phases and phase transformations in the sintered alloys are built. It has been found that changes in the deformation parameters of the porous titanium nickelide*-based *alloys correlate with an increase in the volume fraction of the* TiNi phase and *with its wholeness as the sintering time is increased.*

Keywords: porous titanium nickelide alloy, Ti–Ni system, reaction sintering, liquid-phase sintering, shape memory, TiNi phase, scanning electron microscopy, x-ray spectral microanalysis.

Porous titanium nickelide produced by reaction sintering is known to have extremely inhomogeneous structure and chemical composition, which is characteristic of this powder metallurgy technique [1]. A major fraction of the inhomogeneities is related to the incompleteness of transformation during reactive synthesis. The structural-phase inhomogeneity of the sintered alloy is particularly high in the solid-phase sintering stage. A rise in sintering temperature changes the sintered system from the solid- to the liquid-phase stage, improving the homogeneity of the product. However, the increase in temperature is limited by a concurrent growth of pores and shrinkage of the sample. This effect appears to be undesirable. The problem of producing a high-porosity titanium nickelide alloy by reaction sintering boils down to finding an optimum combination of temperature, exposure time, pore size, and phase homogeneity of the alloy. The major generalized sintering quality indices include the retention of the shape of primary powder particles and the degree of reflow of the porous alloy surface on sintering. With an optimum combination of the above-mentioned parameters, the emergence of the melt causes a dramatic acceleration of mass transfer processes thus increasing the strength of the sample. Notably, to minimize the shrinkage of the sample, growth of pores, and intragranular liquation of the alloy, the amount of the melt must be at a minimum.

In reaction sintering of the Ti–Ni system, the lowest-melting component is the Ti_2Ni phase whose melting stimulates the development of the liquid-phase sintering stage triggering the reaction-diffusion interactions. This gives rise to large pores [2, 3]. In addition to the TiNi phase envelopes formed at the solid-phase stage, there appears another TiNi phase of spongy form at the liquid-phase stage. The latter phase may have a significant effect on the physical-mechanical properties of the sintered alloy.

The object of this work is to study the structure of and the mechanisms involved in the formation of the TiNi phase in reaction sintering of the Ti–Ni system as functions of the exposure time (1.5–3 hrs) and of the extent to which the exposure affects the physical-mechanical characteristics of the high-porosity sintered alloy. The shape-memory

[1]Scientific Research Institute of Medical Materials and Shape-Memory Implants of the V. D. Kuznetsov Physical-Technical Institute at National Research Tomsk State University, Tomsk, Russia; [2]University of Ulsan, Ulsan, South Korea, e-mail: nii_mm@sibmail.com. Translated from Izvestiya Vysshikh Uchebnykh Zavedenii, Fizika, No. 10, pp. 15–21, October, 2014. Original article submitted April 8, 2014.

effect and the superelastic behavior of titanium nickelide-based alloys are of the greatest interest in this study. Also investigated here is the influence of the structural features of the TiNi phase of the porous alloys under consideration on the repeated shape-memory effect. Finally, a comparative analysis is performed between the measurement results for the specific electrical resistance and the literature data about monolithic shape-memory alloys.

TEST MATERIALS AND INVESTIGATION TECHNIQUES

Three groups of cylindrical samples of a porous titanium nickelide alloy measuring 8 × 52 mm were produced in quartz moulds in an electric vacuum furnace, using the reaction sintering technique. The mixture components were PTEM titanium and PNK–OT4 nickel powders (Russian classification). An obligatory sintering condition was preparation of high-porosity samples. The sintering temperature found experimentally was <950°C. In view of the need to retain high porosity of the samples, only the Ti_2Ni phase was allowed to melt, in order to produce melt and initiate liquid-phase interaction without shrinkage of the specimen [4]. In sintering the samples of the first group, the alloys were heated to a maximum temperature and then cooled down to room temperature. The samples of the second and third groups were held at maximum temperatures for 90 and 180 min, respectively. The structure of the porous samples was examined with the use of microsection metallographic specimens prepared by standard metallographic techniques [5]: light microscopy (Axiovert 40 Mat} and scanning electron microscopy (PHILIPS SEM 515). The phase composition was determined by means of an EDAX ECON IV microanalyzer.

The sintered porous cylindrical samples were cut into 35 × 7 × 1 mm plates, using the electrical erosion technique. The repeated shape-memory effect was investigated by a stress-strain test in the bending mode which provided reliable recording of changes in the residual and irreversible deformations of the samples, allowing for estimation of the parameters of the repeated shape-memory effect and changes in the structure of the reaction sintering product. A major portion of the curve for the temperature dependence of the entire multiphase specimen accounts for the complex deformation of a narrow alloy component – the TiNi phase undergoing a reversible phase transformation under the action of temperature and loading.

AN ANALYSIS OF THE RESULTS

An analysis of the structure of the porous samples subjected to sintering for different exposure times enabled us to reveal some general features of the process. The latter was divided into solid-phase and liquid-phase stages.

The Solid-Phase Sintering Stage

On sintering at a maximum temperature of 950°C and for zero exposure time, the porous alloys are extremely structured, which makes it possible to represent the structure as repetitive reaction cells and identify five structural components of the cells (Fig. 1*a*), where the reaction cell core is formed by Ti_β-base solid solution (*1*), a continuous core envelope is formed by the Ti_2Ni phase whose thickness is ≤20μm (*2*), a continuous envelope is formed by the TiNi phase (*3*), the islets on the outer surface of the TiNi envelope are formed by the $TiNi_3$ phase (*4*), and the outer spongy reaction cell envelope formed by Nγ solid solution exhibits certain features (*5*, see Table 1 below). Every so often the titanium core (Fig. 1*b*) consists of several parts (*1*) separated by dendrites (*6*) and envelope (*2*). The core may also be formed by the Ti_β + Ti_2Ni eutectoid or by the Ti_2Ni intermetallic compound alone. Open asymmetric cells are observed (Fig. 1*a*) along with enclosed symmetric cells.

It may be concluded on the basis of currently available concepts of reaction sintering [2, 6] and our experimental data that even with a minimum exposure , reaction cells consisting of three intermetallic envelopes (Ti_2Ni, TiNi, and $TiNi_3$) and two solid solutions (Ti_β and N_γ) are formed as the result of the interdiffusion of the titanium particle into surrounding nickel particles. The solid Ti_β solution that forms a monolithic reaction cell core and contains up to 10 at.% Ni suffers an isothermal decay followed by transformation into the Ti_2Ni +Ti_β eutectoid or stays in a metastable state. In the solid N_γ solution that forms the porous periphery of the reaction cell, the titanium content

TABLE 1. The Concentrations of the Phase Components

Serial number	Phase	Concentration* Ni, at.%
1	Ti core Ti_{β}	9.7
2	Envelope approaching the stoichiometry of Ti_2Ni	35.4
3	Envelope approaching the stoichiometry of TiNi	54.3
4	Envelope with $TiNi_3$ islets	76.3
5	Spongy array close to Ni_{γ}	98.8
6	Dendrites approaching the stoichiometry of Ti_2Ni	32.3
7	Grain-boundary phases close to Ti_{β}+Ti_2Ni eutectoid	30.0
8	Ti_{β} grain body	7.5
9	Transition zone	–
10	Granulation region	–
11	Dendritic region	–
12	Dark gray phase within transition zone	37.55
13	Light gray phase within transition zone	49.80

*Note that the balance is titanium.

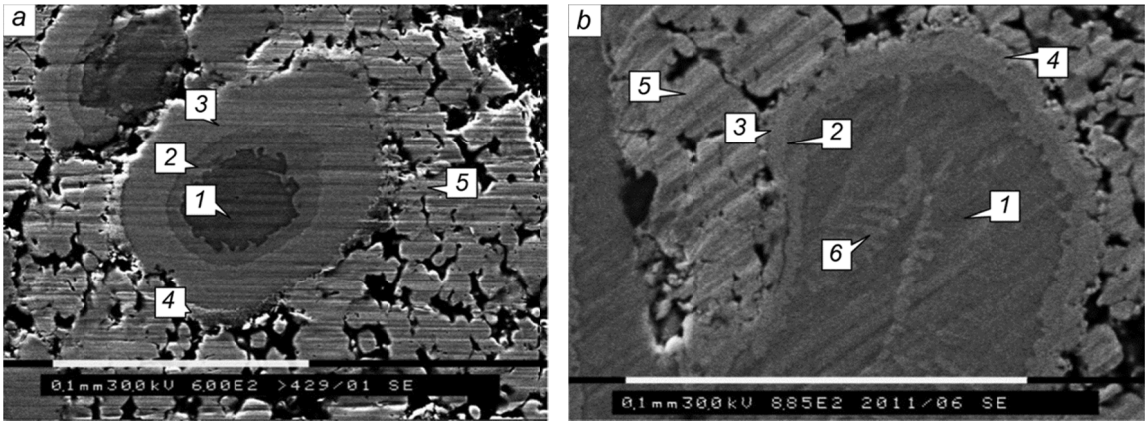

Fig. 1. Reaction cells in the structure of samples at the solid-phase sintering stage: an enclosed symmetric reaction cell (*a*) and a symmetric reaction cell with a composite titanium core (*b*).

varies between 0.6 and 3.0 at.%. The Ti_2Ni phase envelope is formed due to nickel diffusion from the spongy nickel array across the resultant reaction products which hinder further nickel diffusion [7].

The outer spongy envelope of the reaction cell formed by the solid N_{γ} solution has nonuniform density. The spongy envelope of the reaction cells is less dense on the periphery of the sample than in the central zone. According to diffusion mass transfer theory [8, 9], the contact neck growth occurs with high degrees of strain of the nickel particles. The latter process reduces the interparticle pore size in the central part of the sample. For instance, the average interparticle pore size in the spongy envelope on the periphery of the sample is ~150 μm, whereas in the central part, it is as small as ~0.5–1 μm. It should be noted that the interparticle pore size averaged over the entire sample is 12 μm.

Intense heat removal from the periphery of the sample is responsible for the reduced temperature on the periphery and hence for the retention of large interparticle pores. Sintering in the Ti–Ni reaction system is due to the total heat from the main source that serves as a furnace heater and from an additional internal source – an exothermic intermetallic compound synthesis reaction. The temperature of the sintered system is higher than the ambient temperature due to an exothermic addition, and there is heat withdrawal from the surface of the sample. The sintered system is divided into a hotter central zone where the structure of the sample is not affected by the heat

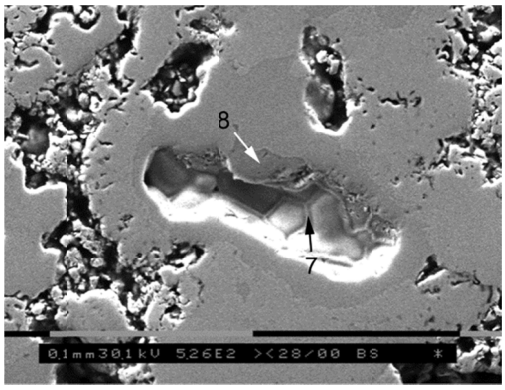

Fig. 2. Microphotographs of the secondary structure: the general view of the central pore upon melting of the reaction cell core.

flow from the center to the periphery and a colder peripheral zone where the heat flow effect makes itself evident in larger pores of the alloy because there is not enough heat in this zone to provide compaction of nickel particles.

In response to the reaction diffusion of titanium into small nickel particles adjacent to a large titanium particle, the titanium content in the particles amounts to ~25 at.% in accordance with the stoichiometric composition of the $TiNi_3$ intermetallic compound. The titanium concentration decreases down to 1–3 at.% and corresponds to that of the N_γ solid solution even in the next row of the nickel particles out of contact with the titanium particle. The discontinuous change in the titanium concentration is attributable to abrupt termination of the diffusion flow induced by the detachment of particles adjacent to titanium from the rest of the spongy nickel array because of the particle shrinkage. The latter is in turn caused by the appearance of the $TiNi+TiNi_3$ eutectic at the boundary with the TiNi phase envelope and by a local increase in temperature above 1100°C by virtue of the exothermicity of the $TiNi + Ni \rightarrow TiNi_3$ phase transformation.

The Liquid-Phase Sintering Stage

An increase in the exposure time to 90 min at a temperature of ~950°C causes the lowest-melting-point component − Ti_2Ni phase –to melt and, according to modern views on liquid-phase sintering, brings about a qualitative change of the sintering process from the solid-phase stage to that of the liquid-phase to form a secondary structure. The transition intensity is determined by the rates of Ti_2Ni phase melting, capillary spreading of the melt, and dissolution of the TiNi, Ti_β, N_γ, and $TiNi_3$ phases in the melt. In this case, the secondary structure loses regularity inherent in the primary structure, and the pores in the sintered system change drastically: one type of the interparticle pores found in the primary structure gives way to three types of pores formed in the secondary structure. Let us examine the three types of pores observed in the structures under study.

Type 1 is central pores of size 30–70 μm formed where the reaction cell core was located (Fig. 2) as a result of the melting of the Ti_2Ni phase and concurrent dissolution of the Ti_β phase. Part of the melt is absorbed by the TiNi envelope to form a titanium-rich zone there. The latter is responsible for the development of the secondary Ti_2Ni phase on crystallization. The central pores often contain the remains of the titanium core in the form of grains *8* of envelope *7* (see Table 1).

Type 2 is circular pores formed between the intermetallic TiNi envelope and the core as a result of the melting of the Ti_2Ni phase and partial dissolution of the titanium core.

Type 3 is tortuous pores formed in the spongy array in consequence of interaction between the N_γ solid solution and the Ti_2Ni phase melt. Spreading over the spongy array under the action of capillary forces, the melt partially dissolves the array. Thereafter the residual phase retains its morphology, but the concentrations of its constituents become inhomogeneous. In places, the concentrations approach those of TiNi or $TiNi_3$. The average size of the tortuous pores in the secondary structure increases to ~25 μm due to partial melting and capillary spreading of the spongy nickel

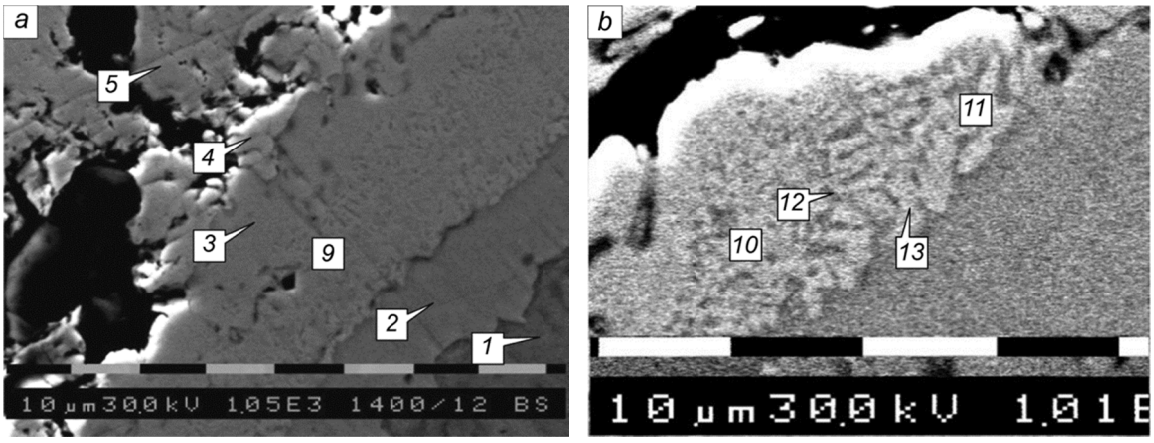

Fig. 3. Microphotographs of fragments of the Ti_2Ni–TiNi transition zone in a reaction cell: the general view of the transition zone (*a*) and granulation and dendritic regions (*b*).

array. The foregoing conjectured processes are quite compatible with the liquid-phase sintering principles described elsewhere [9–11].

The diffusion transition zone (Fig. 3) consists of granulation *10* and dendritic regions *11*. The respective width of the regions is 3–11 and 4–10 μm. The composition of dark gray phase *12* is $Ni_{38}Ti_{62}$, which corresponds to the (Ti_2Ni+TiNi) region in the phase diagram of the Ti–Ni system within the transition zone. The light gray phase *13* – $Ni_{50}Ti_{50}$– corresponds to the TiNi homogeneity region. The titanium nickelide phase *1* formed at the solid-phase sintering stage as a result of the solid-phase reaction of the Ti and Ni powders interacts with the Ti_2Ni phase melt *2* at the liquid-phase sintering stage during a 3 hour exposure, which gives rise to a 5–17 μm wide transition zone on the periphery of the TiNi phase. Interaction of the melt of Ti_2Ni phase *2* with the envelope of primary TiNi phase *3* at the liquid-phase sintering stage gives rise to the 5–20 μm wide transition zone *9* (Fig. *3a*).

As the transition zone is crystallized, the solid TiNi phase interacts with the surrounding Ti_2Ni melt by the peritectic mechanism. As this takes place, two oppositely directed processes are found to develop: (1) dendritic branching favorable to a decrease in the concentration supercooling and (2) isothermal structural coarsening (the Gibbs−Thomson effect) due to surface diffusion. A high concentration gradient before the crystallization front of dendritic branches is responsible for the instability of crystallization during which the composition and the quantitative relationship between dendrites and melt of the transition zone undergo changes [12, 13].

The Repeated Shape-Memory Effect Under Loading

The repeated shape-memory effect in TiNi-based alloys is defined as a phenomenon involving a repeated change in the shape of the material brought about by a change in its phase state owing to varying temperature of the system both in heating and in cooling. Different martensite transformation sequences taking place in the alloys also predetermine singularities of manifestation of the repeated shape-memory effect. An analysis of experimental relationships associated with the effect observed in a series of the porous titanium nickelide-based samples employed findings of the article [4] where monolithic alloys had been studied and a combined examination of the x-ray diffraction data and temperature dependence of macrodeformation under loading had been performed. As a result, we have determined a phase transformation sequence taking place in the temperature range –196 − +200°C. In addition, a comparative analysis was made of the experimental dependence of the repeated shape-memory effect for the porous sample sintered with a 1.5-hour exposure (Fig. 4) and the one known for a cast $Ti_{50}Ni_{48}Fe_2$ alloy (Fig. 5). The experimental curves were divided into portions, much like in the familiar dependence, and the portions were related to the phase transformation sequences found for the monolithic alloy. Inflections of the curve for the repeated shape-

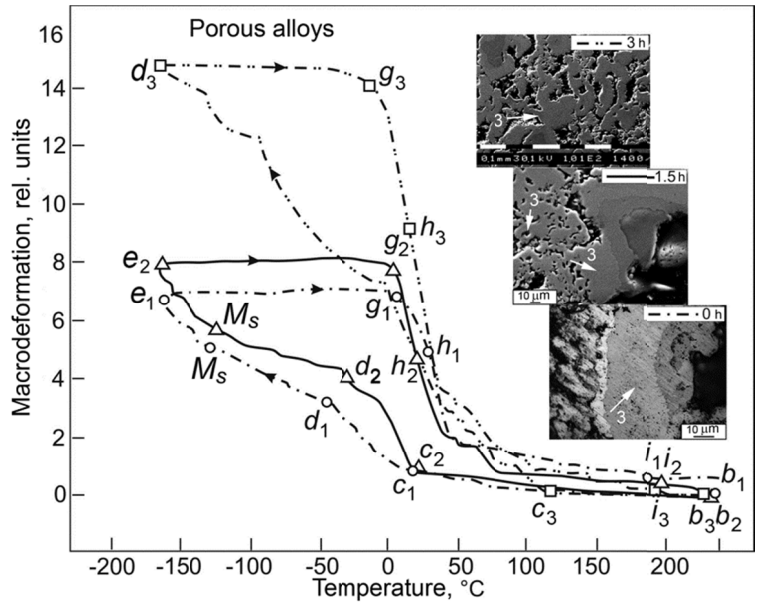

Fig. 4. Repeated shape-memory effect under permanent loading and porous sample microstructure subjected to sintering with 0, 1.5-, and 3.0-hour exposures.

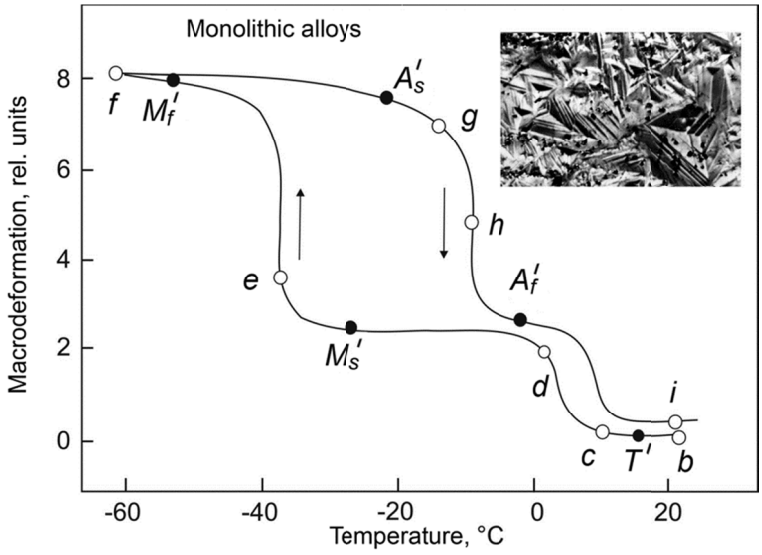

Fig. 5. Schematic representation of the repeated shape-memory effect $B2 \leftrightarrow R \leftrightarrow B19'$ in the monolithic $Ti_{50}Ni_{48}Fe_2$ alloy under loading.

memory effect in portions b–M_s and h–i are evidence of the fact that both the forward and the reverse martensite transformations $B2 \leftrightarrow R \leftrightarrow B19'$ develop in two stages [4].

The above-indicated portions of the curves for the repeated shape-memory effect in the porous and monolithic samples exhibit certain similarities and differences. In the curve for the porous alloy, two portions inherent in the cast alloy are lacking. This is due to the incompleteness of the phase transformation characteristic of porous titanium nickelide alloys [14]. Missing are the portions e–f and f–g marked by alternate formation and disappearance of the R-phase in the cast alloy and by a noticeable growth and predominance of the $B19'$ phase. From this it may be inferred

TABLE 2. The Shape-Memory Effect Parameters for Porous Samples Produced with Different Exposure Times

Shape-memory effect parameters	Exposure, h		
	No exposure	1.5-hour exposure	3-hour exposure
Temperature hysteresis $\Delta T_{B2\leftrightarrow R}$, °C	130	66	42
Temperature hysteresis $\Delta T_{R\leftrightarrow B19}$, °C	182	167	152
Accumulated strain, rel. units	6.3	7.8	13.8
Residual strain, rel. units	0.81	0.74	0.52

that in the porous alloy of interest, the amount of the *R*-phase decreases late in the forward transformation, whereas the growth of the *B*19′ phase slows down and its amount gets much smaller than in the cast alloy.

The temperature hysteresis $\Delta T_{R\leftrightarrow B19'}$ determined graphically from the temperature dependence of the repeated shape-memory effect for the sample subjected to sintering with a 1.5-hour exposure is 120−150°C, whereas for the $Ti_{50}Ni_{48}Fe$ alloy, it is 30°C. For the $B2\leftrightarrow R$ transition, the temperatures are between 42 and 130°C, and for the $R\leftrightarrow B19$ transition, the temperature range is152–182°C (see Table 2).

Accumulation of strain during the forward $B2\rightarrow R\rightarrow B19'$ transformation occurs slower than it takes the sample to recover its shape (Fig. 5) during the reverse $B19'\rightarrow R\rightarrow B2$.transformation. This enables us to assign the forward transformation kinetics to the athermic type characteristic of the class II phase transitions according to Tong and Wayman, while the reverse transformation kinetics is classed with the explosive type inherent in the class I transitions [15]. In the sample subjected to sintering with a 3-hour exposure, the branch of the forward transformation in the temperature dependence of the repeated shape-memory effect comes to correspond to the athermic transformation kinetics even to a greater degree. We failed to identify portions of the temperature curves characteristic both of the $B2\rightarrow R$ and of the $R\rightarrow B19'$transformations in the segment of the sample undergoing the forward b_3–d_3 transformation because high-temperature and low-temperature phases are present in the porous alloy in the entire temperature range –196 – +200°C wherein the phase transformations take place [4]. Summarizing the foregoing discussion, it can be said that the transformation temperature ranges get wider for the porous alloys because of the inhomogeneous concentration and phase of the sintering product. The structural inhomogeneity is amplified by the extremely nonuniform loading of highly porous samples. In this case, quite a few segments of the sample are found in a tensile or a compressive, or else in a bending states simultaneously.

It is evident from maximum and residual strain distributions as a function of sintering time (Table 2) that the lowest degree of accumulated strain (6.3 rel. units) is observed in the sample subjected to sintering using a zero exposure. This is related to the highest degree of isolation of the TiNi phase between the Ti_2Ni phase envelopes and the spongy Ni array within each of the reaction cells (Fig. 5). An increase in the maximum accumulated strain from 7.8 to 13.8 rel. units with increase in the exposure time from 1.5 to 3 hours is connected with formation of the additional spongy component of the TiNi phase due to interaction of spongy nickel with the Ti_2Ni phase melt.

The variation in the temperature hysteresis of the $B2\leftrightarrow R$ and $R\leftrightarrow B19$ transitions exhibits a different pattern, decreasing with increase in the exposure time, which is particularly noticeable for the $R\leftrightarrow B19$ transition (see Table 2). Temperature hysteresis is characteristic of the nondiffusion $R\leftrightarrow B19$ transition, whereas the $B2\leftrightarrow R$ transition has no temperature hysteresis [4]. This is readily demonstrated by the $Ti_{50}Ni_{48}Fe_2$ alloy. In the porous alloy, the dependence has a different form (see Fig. 5), which is attributable to the mixed type of the transition for which the $B2\rightarrow R$ and $R\rightarrow B19$ transformations do not occur consecutively for a small number of growth centers; rather they develop simultaneously for a large number of growth centers, interacting with each other. This is why it is difficult to identify portions of the curve for the temperature dependence in the $B2\rightarrow R$- and $R\rightarrow B19$ transitions. Notably, these portions are well discernible in the cast alloy (see Fig. 5). The reverse $B19\rightarrow R\rightarrow B2$ transformation in all the samples occurs approximately in the same temperature range. However, because of increased exposure time and TiNi phase increment owing to the spongy component, the temperature range for the forward $B2\rightarrow R$ transformation is shifted, decreasing temperature hysteresis. As a result, the temperature hysteresis at the first and second stages of the familiar dependence for the $Ti_{50}Ni_{48}Fe_2$ alloy [4] is ~5–25°C, whereas in the porous samples obtained in this work, the temperature hysteresis is ~50–130°C.

CONCLUSIONS

We have investigated the problems of reaction sintering of titanium-nickelide-based alloys exhibiting the shape-memory effect and arrived at the following conclusions.

1. For reaction sintering of PNK-OT4 Ni and PTEM Ti powders (Russian classification), the maximum sintering temperature and exposure time are found to be 950°C and 3 hrs, respectively. Under these conditions, an optimum combination of the porosity and structural-phase composition of the alloy as well as of the repeated shape-memory effect involved in the material was obtained.

2. As a result of melting the Ti_2Ni phase at a temperature of 950°C and a change of the sintering process from the solid-phase stage to the that of the liquid-phase, large pores are formed in the reaction cell core. Solid-liquid interaction of melt and spongy nickel array gives rise to an additional TiNi phase in which a transition zone with dendritic structure arises.

3. An increase in the sintering time causes the volume fraction of the secondary TiNi phase to increase. Owing to this, the maximum accumulated strain of the samples increases, whereas thermal hysteresis of the dependence of the shape-memory effect decreases.

REFERENCES

1. V. V. Skorokhod and S. M. Solonin, Physical-Metallurgical Fundamentals of Sintering of Powders [in Russian], Metallurgiya, Moscow (1984).
2. M. Whitney, S. F. Corbin, and R. B. Gorbet, Acta Mater., **56,** No. 3, 559 (2007).
3. N. V. Artyukhova, A. N. Monogenov, Yu. F. Yasenchuk, and V. E. Gunther, Russ. J. Non-Ferrous Metals, **53**, No. 1, 95–100 (2012).
4. V. E. Gunther, V. N. Khodorenko, Yu. F. Yasenchuk, *et al*., Titanium Nickelide. A New Generation Medical Material [in Russian], MITs Publishing House, Tomsk (2006).
5. E. Becker, J. Kerster, G. Freyer, L. Frolich, Practische Fragen zur Prufung von Metallen [Russian translation], Metallurgiya, Moscow (1979).
6. V. Yu. Filimonov, Polzunov. Vestrnik, No. 4−1, 36 (2005).
7. A. P. Aldushin, A. G. Merzhanov, and B. I. Haikin, Dokl. Akad. Nauk SSR, **204**, No. 5, 1139–1142 (1972).
8. P. Weller and H. Exner, Phys. Sintering, **5**, No. 2/2, 25–37 (1973).
9. A. P. Savitskii, Liquid-Phase Sintering of Systems with Interacting Components [in Russian], Nauka, Novosibirsk (1991).
10. G. A. Libenson, Fundamentals of Powder Metallurgy [in Russian], Metallurgiya, Moscow (1987).
11. B. B. Straumal, Phase Transitions at Grain Boundaries [in Russian], MISiS, Moscow (2004).
12. Merton C. Flemings, Solidification Processing, McGraw Hill Book Company, New York (1974).
13. V. I. Dobatkin, V. I. Dobatkin Selected Scholarly Work [in Russian], VIlS, Tech. Phys. Lett., **27**, No. 11, 970–972 (2001).
14. H. C. Tong, Acta Metall., **22**, No. 7 (1974), p. 887.